

Direction reversal of non-Hermitian skin effect via coherent coupling

Linhu Li,^{1,*} Wei Xin Teo,^{2,†} Sen Mu,^{2,‡} and Jiangbin Gong^{2,‡}

¹Guangdong Provincial Key Laboratory of Quantum Metrology and Sensing & School of Physics and Astronomy, Sun Yat-Sen University (Zhuhai Campus), Zhuhai 519082, China

²Department of Physics, National University of Singapore, Singapore 117551, Republic of Singapore
(Dated: March 16, 2022)

Absolute negative mobility (ANM) in nonequilibrium systems depicts the possibility of particles propagating toward the opposite direction of an external force. We uncover in this work a phenomenon analogous to ANM regarding eigenstate localization and particle transport in non-Hermitian systems under the influence of the non-Hermitian skin effect (NHSE). A coherent coupling between two non-Hermitian chains individually possessing the same preferred direction of NHSE is shown to cause a direction reversal of NHSE for all eigenmodes. This concept is further investigated in terms of time evolution dynamics using a non-Hermitian quantum walk platform within reach of current experiments. Our findings are explained both qualitatively and quantitatively. The possible direction reversal of NHSE can potentially lead to interesting applications.

Introduction. - Non-Hermitian Hamiltonians provide an effective description of open quantum systems or wave systems with gain and loss [1–4]. One main feature of non-Hermitian lattice systems with nonreciprocity is the seminal non-Hermitian skin effect (NHSE) under open boundary conditions [5–8]. NHSE causes directional accumulation of eigenmodes at the system’s boundaries and has a rather deep connection with the point-gap topology of the complex spectrum of non-Hermitian systems [5–17]. NHSE has spurred considerable interest in condensed matter physics research because it challenged our conventional thinking of bulk-edge correspondence and has motivated the so-called non-Bloch band theory [6–8]. Much attention has also been paid to the interplay between the NHSE and other important physical effects, such as topological localization [14, 15], external electromagnetic fields [18–20], disorders and defects [21–29].

Non-reciprocal hopping on a one-dimensional (1D) lattice defines a preferred direction analogous to a physical direction of an external force. The preferred boundary for bulk state localization as NHSE is thus intuitive, so does the preferred direction favoring particle transport [10, 15, 17, 30–34]. For example, if the strength of intercell hopping to the left is always larger than that to the right, then NHSE is expected to localize all states at the left boundary. On the other hand, we must take note of one remarkable dynamical phenomenon, namely, absolute negative mobility (ANM), where particles propagate toward the opposite direction of an external force. Seemingly contradictory to Newton’s second law, ANM has already been widely investigated and experimentally realized in various systems far from equilibrium [35–45]. Recognizing non-Hermitian systems as nonequilibrium systems, it is necessary to address the possibility of population accumulation or particle transport in a direction against the preferred direction indicated by the non-reciprocal hopping. This issue is not only of theoretical interest, but may offer versatile control knobs to manipulate NHSE for various applications, such as light funneling [46] and directional signal amplification [30, 31, 47].

In this work, we unveil a general scheme to induce 1D NHSE in a direction precisely opposite to the favored direction of non-reciprocal hopping. As shown below, this exotic

phenomenon can be obtained at both the eigenstate level and the dynamics level. There can be multiple interpretations of why a direction reversal of NHSE occurs. Among them, a simple physical picture adopted below is based on the interference between multiple hopping pathways. Specifically, if two non-Hermitian lattices with the same preferred non-reciprocal direction are coupled, then multiple hopping pathways become available. The resulting interference between the multiple hopping pathways can counter-intuitively and drastically alter the effective strengths of hopping towards two directions, and hence one must reexamine the true physically favored direction of NHSE.

The direction reversal of NHSE by coherent coupling is in principle observable in a variety of quantum and classical platforms realizing NHSE [32–34, 46, 48–52]. In particular, reversed NHSE at the eigenstate level is already within the reach of classical platforms, such as circuits. However, how reversed NHSE is manifested at the dynamics level is less straightforward. We hence propose a non-unitary quantum walk setting directly addressing non-Hermitian dynamics [32–34], with the essential addition being an interchain hopping for the quantum walker along two chains. As elaborated below, even though the preferred direction of NHSE is no longer obvious in the quantum walk dynamics, the multiple propagation pathways induced by the interchain hopping can still lead to a direction reversal of particle transport.

Direction reversal of eigenstate population accumulation. - Our starting point is a minimal model depicting two coupled non-Hermitian chains [53] with different on-site potentials, as shown in Fig. 1. The real-space Hamiltonian reads

$$\hat{H} = \sum_{x=1}^L \sum_{s=a,b} \left[t_s e^{\alpha_s} \hat{s}_x^\dagger \hat{s}_{x+1} + t_s e^{-\alpha_s} \hat{s}_x^\dagger \hat{s}_{x-1} + t_\perp (\hat{a}_x^\dagger \hat{b}_x + \hat{b}_x^\dagger \hat{a}_x) + \mu_a \hat{a}_x^\dagger \hat{a}_x + \mu_b \hat{b}_x^\dagger \hat{b}_x, \right] \quad (1)$$

with t_s and $\alpha_s > 0$ determining the asymmetric hopping amplitudes on the two chains labeled by $s = a, b$. Referring to Fig. 1, the preferred direction of the non-reciprocal hopping here is apparently to the left for both chains. The on-site potential is set to be $\mu_a = -\mu_b = \mu$, with all other choices being

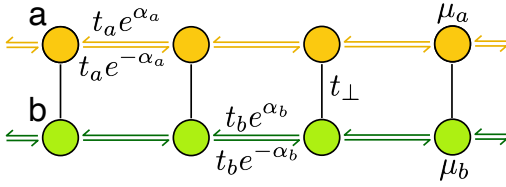


FIG. 1. Schematic of two coupled chains with non-reciprocal hoppings. In either lattice, the amplitude of hopping to the left direction is $t_s e^{\alpha_s}$ ($s = a, b$), apparently with a magnitude larger than that to the right direction $t_s e^{-\alpha_s}$. t_\perp introduces coupling between the two chains and hence multiple hopping pathways from one lattice site to its neighboring site.

equivalent upon shifting their eigenenergies. The two chains are completely decoupled if $t_\perp = 0$, each displaying NHSE localization at the left edge, with an inverse localization length $\kappa_{a,b} = \alpha_{a,b}$ [6, 8, 14]. An example depicting such a decoupling limit is illustrated in Fig. 2(a).

Upon switching on the interchain coupling ($t_\perp \neq 0$), both the complex spectrum and eigenstate localization of the coupled system start to differ from that of the uncoupled case, no matter how small t_\perp is [16, 54, 55]. To allow for many hopping pathways from one site to its neighboring site, such as $a_x \rightarrow a_{x+1}$ and $a_x \rightarrow b_x \rightarrow b_{x+1} \rightarrow a_{x+1}$, to interfere significantly, here we investigate a strong coupling regime with sufficiently large t_\perp . It is then found that *all* eigenmodes can now localize at the opposite edge as compared with that in the uncoupled case. This is clearly seen in Fig. 2(a)-(c) as the interchain coupling strength t_\perp increases from 0 to 6 and to 15.

To characterize the above-observed direction reversal of NHSE, we consider averages of the standard and directional inverse participation ratios (IPR and dIPR), defined as

$$\bar{I} = \frac{1}{2L} \sum_m \sum_{x=1}^L (|\psi_{x,m}^a|^4 + |\psi_{x,m}^b|^4), \quad (2)$$

$$\bar{I}_d = \frac{1}{2L} \sum_m \sum_{x=1}^L \frac{(x - (L+1)/2) (|\psi_{x,m}^a|^4 + |\psi_{x,m}^b|^4)}{(L-1)/2}, \quad (3)$$

with $\psi_{x,m}^s$ the wave amplitude of the m -th normalized right eigenmode at site x of sublattice s . Representative results are presented in Fig. 2(d). It is seen that the IPR (and the absolute value of dIPR) gets larger either for weaker or stronger t_\perp , indicating a stronger boundary accumulation of the eigenmodes, but with opposite accumulating directions, as evidenced by the signs of the dIPR. A reversal of the NHSE direction starts to occur when $\bar{I}_d = 0$, which is at $t_\perp \approx 6.3$ in the shown example. In the neighborhood of the transition point $\bar{I}_d = 0$ [see Fig. 2], the eigenmodes can possibly localize at both boundaries in a balanced manner as the bipolar NHSE [56, 57]. More importantly, away from the transition point, *all* eigenmodes are now localized at the opposite boundary as compared with the uncoupled case. Meanwhile, the difference between the average distribution on the two lattices, defined

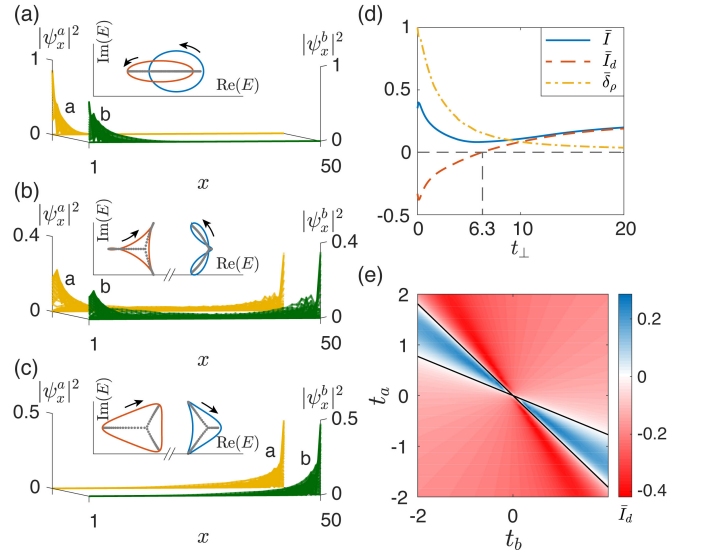


FIG. 2. (a-c) Distribution of all eigenmodes on the two chains, with different interchain coupling $t_\perp = 0, 6, 15$ respectively. Insets show the corresponding spectra under PBC (red and blue for the two bands) and OBC (gray). Clockwise and anti-clockwise winding directions of the PBC spectra versus the quasi-momentum k , as indicated by the black arrows, correspond to OBC skin modes localized on the left and right, respectively [11–13]. Note that in (b) and (c), we have omitted a large spacing in $\text{Re}[E]$ between the two energy bands (red and blue), represented by the double slash in the axis. Other parameters are $t_a = 0.75$, $t_b = -1$, $\alpha_a = 0.5$, $\alpha_b = 0.2$, and $\mu_a = -\mu_b = 0.5$. (d) \bar{I} , \bar{I}_d , and $\bar{\delta}_\rho$ defined in Eqs. (2), (3) and (4), versus the interchain coupling t_\perp , with the same parameters as in (a-c). (e) Phase diagram regarding the directional IPR \bar{I}_d at $t_\perp = 30$ with other parameters the same as (a-c). Black lines are obtained from the perturbation results of Eq. (8).

as

$$\bar{\delta}_\rho = \frac{1}{2L} \sum_m \left| \sum_{x=1}^L (|\psi_{x,m}^a|^2 - |\psi_{x,m}^b|^2) \right|, \quad (4)$$

is seen to decrease with increasing t_\perp , indicating a stronger hybridization between the two chains at larger t_\perp .

Physics of reversed NHSE.— To confirm that the main physics behind reversed NHSE is the interference between multiple hopping pathways, we consider a straightforward first-order perturbation theory by treating $\hat{H}_\perp = t_\perp \sum_x (\hat{a}_x^\dagger \hat{b}_x + \hat{b}_x^\dagger \hat{a}_x)$ as the unperturbed Hamiltonian. The unperturbed eigenmodes at site x are simply given by local hybridized adiabatic modes of the coupled system, i.e.,

$$|u_{\pm,x}\rangle = \hat{u}_{\pm,x}^\dagger |0\rangle = (\hat{a}_x^\dagger \pm \hat{b}_x^\dagger) |0\rangle / \sqrt{2}, \quad E_{\pm,x} = \pm t_\perp, \quad (5)$$

with $|0\rangle$ the vacuum and $E_{\pm,x}$ the corresponding unperturbed eigenenergies due to the coherent coupling. By taking all the rest terms as a perturbation, we rewrite the non-reciprocal hopping Hamiltonian in the local adiabatic representation,

yielding

$$\hat{H}'_{\pm} = \sum_x (t_a e^{\alpha_a} + t_b e^{\alpha_b}) \hat{u}_{\pm,x}^{\dagger} \hat{u}_{\pm,x+1} + (t_a e^{-\alpha_a} + t_b e^{-\alpha_b}) \hat{u}_{\pm,x+1}^{\dagger} \hat{u}_{\pm,x} + (\mu_a \pm \mu_b) \hat{u}_{\pm,x}^{\dagger} \hat{u}_{\pm,x}. \quad (6)$$

Interestingly, other than the local on-site energy being expectedly different, the “+” and “-” hybridized lattice sites have the same non-reciprocal hopping strengths, $(t_a e^{\alpha_a} + t_b e^{\alpha_b})$ to the left and $(t_a e^{-\alpha_a} + t_b e^{-\alpha_b})$ to the right. That is, the effective hopping amplitudes are seen to be a sum of two individual hopping amplitudes $t_a e^{\alpha_a}$ and $t_b e^{\alpha_b}$ or $t_a e^{-\alpha_a}$ and $t_b e^{-\alpha_b}$, thus clearly indicating an interference mechanism. Most importantly, if t_a and t_b are of different signs, then there is a destructive interference between the two favored amplitudes. This can then lead to

$$|t_a e^{-\alpha_a} + t_b e^{-\alpha_b}| > |t_a e^{\alpha_a} + t_b e^{\alpha_b}|, \quad (7)$$

meaning that NHSE here should accumulate/localize population to the right for *all* the eigenmodes, opposite to the NHSE direction on the uncoupled chains. Inequality (7) also suggests that reversed NHSE occurs within the following parameter regime

$$\frac{t_a}{-t_b} \in \left(\frac{e^{\alpha_b} - e^{-\alpha_b}}{e^{\alpha_a} - e^{-\alpha_a}}, \frac{e^{\alpha_b} + e^{-\alpha_b}}{e^{\alpha_a} + e^{-\alpha_a}} \right), \quad (8)$$

as shown by the solid lines in Fig. 2(e). The transition lines obtained this way match well with the numerical results based on the sign of the average directional IPR \bar{I}_d . A momentum space perturbation theory together with the so-called generalized Brillouin zone [6, 7] yields the same prediction in theory, as detailed in Supplementary Materials. Note also that the role of the on-site potential difference μ is not seen here due to our first-order treatment or the strong coupling assumption. The actual threshold value t_{\perp} to enter the reversed NHSE regime gradually increases with μ . Reversed NHSE may also be obtained under $t_a t_b > 0$, if we introduce multiple hopping pathways in other manners, such as allowing for off-diagonal couplings between the two chains. These details can be found in Supplementary Materials.

Reversed particle transport in non-Hermitian quantum walk. - So far, the reversed NHSE is investigated on the eigenstate level via population accumulation against the preferred direction of non-reciprocal hopping. To make a closer analogy to ANM, it is necessary to explore how this leads to particle transport along a reversed direction. To motivate experimental interest, we use an available and fruitful platform, namely, a discrete-time non-unitary quantum walk model realizing the NHSE through single-photon dynamics in a 1D chain [32–34]. We now propose a quantum walker along two chains, plus a local interchain exchange depending on the spin state.

Specifically, we consider the following two Floquet operators governing the quantum walk,

$$U_0 = R(\theta_1) S_2 R(\theta_2 + \theta_3) M R(\theta_2 + \theta_3) S_1 R(\theta_1), \quad (9)$$

$$U = R(\theta_1) S_2 R(\theta_2) S_4 R(\theta_3) M R(\theta_3) S_3 R(\theta_2) S_1 R(\theta_1). \quad (10)$$

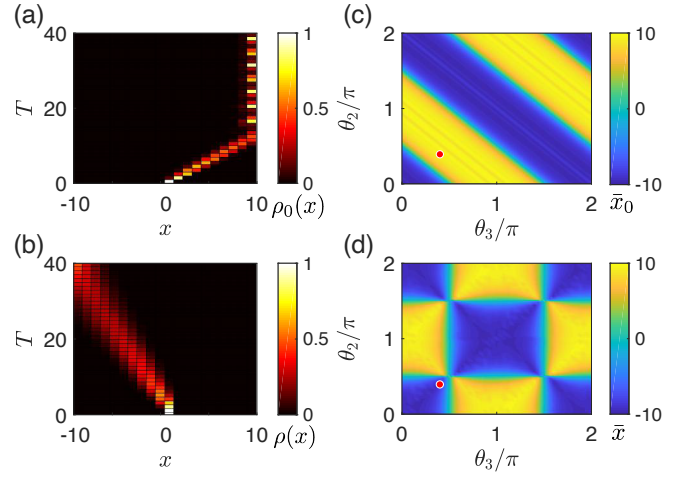


FIG. 3. (a,b) Spatial distributions of the quantum walks for an initial state prepared in the middle of the system, governed by U_0 and U , the two quantum walks without and with the interchain hopping, respectively. (c,d) Average position of the final for the two quantum walks at $T = 40$, versus the two angles θ_2 and θ_3 . Yellow and blue (bright and dark) regimes indicate non-reciprocal pumping toward the directions of $x = N$ and $x = -N$ respectively. The red points in (c,d) represents the two cases of (a,c), with $\theta_2 = \theta_3 = 0.4\pi$. Other parameters are $\alpha_a = \alpha_b = 3$, $\theta_1 = 0.2\pi$ and $N = 10$.

Here $R(\theta)$ rotates the spin by θ about the y axis, with $R(\theta) = \sum_{x=-N}^N \sum_{s=a,b} |s, x\rangle \langle s, x| \otimes e^{-i\lambda_s \theta \sigma_y / 2}$, $s = a, b$ denoting the two chains, x the site index, and $\lambda_a = 1$ and $\lambda_b = -1$. The shift operators S_1 and S_2 are standard quantum walk operations, as they shift the walker to the left and right along either chain, if and only if the spin is up and down, respectively. Non-unitarity/non-Hermiticity is introduced through the operator M , with

$$M = \sum_{x=-N}^N \sum_{s=a,b} |s, x\rangle \langle s, x| \otimes (|\downarrow\rangle \langle \downarrow| + e^{-\alpha_s} |\uparrow\rangle \langle \uparrow|),$$

describing the (quasi-)particle loss only for the spin-up component. U_0 thus defined above yields exactly two copies of the quantum walk model realizing the NHSE in Refs. [32–34], but with opposite spin rotation angles through the parameter λ_s . The M operator alone seems to suggest that the spin-down channel is favored. This effect further interplays with the spin rotation operator $R(\theta)$ and the shift operators $S_{1,2}$ to yield non-reciprocal particle transport, with the preferred direction no longer obvious. Despite the difference in λ_s between the two quantum walk copies, their preferred direction of transport is found to be always the same.

We now couple the two chains accommodating U_0 , thus defining our quantum walk model U . U is obtained by inserting S_3 and S_4 into U_0 . S_3 and S_4 are almost the same operations as S_1 and S_2 except that the walker is instructed to hop onto the other chain (of the same lattice index) when the spin state is up and down, respectively. Detailed definitions of these operations are shown in Supplementary Materials. S_3 and S_4 are expected to hybridize the two chains and

induce interference between multiple hopping pathways. We aim to show that even though the two individual chains have the same preferred walk direction, their coupling can reverse the direction of transport, thus demonstrating direction reversal of NHSE via time evolution dynamics.

We consider an initial state prepared in the middle of the system, $\Psi_{\text{ini}} = \frac{1}{\sqrt{2}}(|a, 0\rangle \otimes |\uparrow\rangle + |b, 0\rangle \otimes |\uparrow\rangle)$. In Fig. 3(a) and (b), we show the spatial distribution $\rho_0(x)$ of the normalized final state $\Psi_{0,\text{fin}} = U_0^T \Psi_{\text{ini}}$ and $\rho(x)$ of $\Psi_{\text{fin}} = U^T \Psi_{\text{ini}}$ for the quantum walk governed by U_0 and U , respectively. Here T represents the number of steps of the quantum walk, and the normalized spatial distribution is defined as $\rho(x) = \sum_{s=a,b,\sigma=\uparrow,\downarrow} |\tilde{\psi}_{\text{fin}}^{x,s,\sigma}|^2$, with $\tilde{\psi}_{\text{fin}}^{x,s,\sigma}$ the wave amplitude of the normalized final state,

$$\tilde{\psi}_{\text{fin}}^{x,s,\sigma} = \frac{\psi_{\text{fin}}^{x,s,\sigma} |s, x\rangle \otimes |\sigma\rangle}{\sqrt{\sum_{x,s=a,b,\sigma=\uparrow,\downarrow} |\psi_{\text{fin}}^{x,s,\sigma}|^2}},$$

obtained from $\Psi_{\text{fin}} = \sum_{x,s=a,b,\sigma=\uparrow,\downarrow} \psi_{\text{fin}}^{x,s,\sigma} |s, x\rangle \otimes |\sigma\rangle$. It is clearly seen from Fig. 3(a) and (b) that introducing the interchain hopping reverses the propagation direction of the walker. In Fig. 3(c) and (d), we further examine the average position of the final state, defined as $\bar{x} = \sum_{x,s=a,b,\sigma=\uparrow,\downarrow} x |\psi_{\text{fin}}^{x,s,\sigma}|^2$. Note that this average is over both chains. Without the interchain hopping operators $S_{3,4}$, the quantum walk governed by U_0 exhibits the NHSE, of which the direction of non-reciprocal population accumulation is determined by the two rotation angles θ_1 and $\theta_2 + \theta_3$ in Eq. (9). As seen in Fig. 3(c) and (d), the interchain hopping can reverse the direction of particle transport. That is, when the color in Fig. 3(c) mismatches that in Fig. 3(d), reversed particle transport, as compared with the decoupled case, occurs. Combining the results in Fig. 3(c) and (d), we obtain the parameter regime in Fig. 4(a) on the $\theta_3 - \theta_2$ plane, where reversed particle transport is observed.

To further digest the direction reversal of NHSE, one may also investigate the winding behavior of the quasi-energy ε_k , obtained from $U_k \Psi_k = e^{-i\varepsilon_k} \Psi_k$, with U_k being the Fourier transform of U , Ψ_k the eigenvectors of U_k , and k the Bloch momentum reflecting the translational invariance of the quantum walk model. The winding of the quasi-energy spectrum as k increases from 0 to 2π is shown in Fig. 4(b) to (f). The direction of the winding is seen to change when the system parameters (θ_2, θ_3) move across the phase boundary identified in Fig. 4(a). There is hence a jump of the spectral winding number between ± 1 and 0, as we go from case (b) to case (f). In particular, as shown in Fig. 4(c) and (e), along the phase boundary, the quasi-spectrum in the k -space does not enclose any area, corresponding to a trivial spectral winding and the absence of NHSE. These results further verify that the above observed reversal of particle transport direction is due to reversed NHSE.

To conclude, we note that particle transport with a reversed direction, as illustrated in Fig. 3(a) and (b), can be observed within very few quantum walk steps. The required lattice size can also be small since there is no need to distinguish between

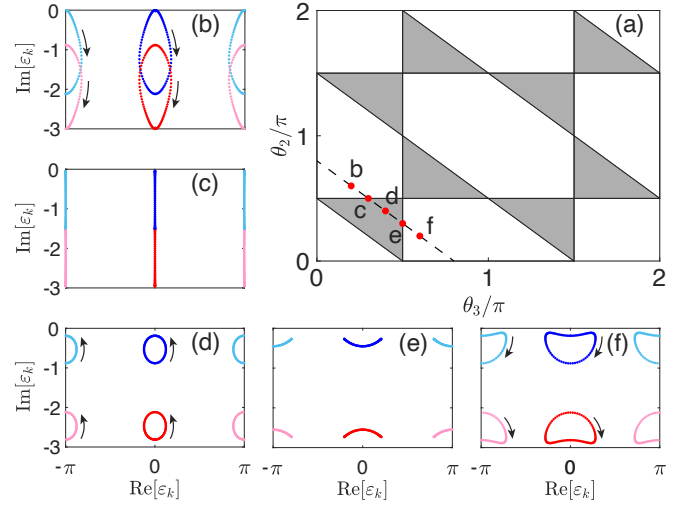


FIG. 4. (a) A phase diagram obtained from Fig. 3(c) and (d), reversed non-reciprocal accumulation occurs for the parameters falling in the gray areas. (b) to (f) The quasi-energy spectra of U_k with different parameters, corresponding to the five red dots along the black dash line with $\theta_2 + \theta_3 = 0.8\pi$ in panel (a). Different colors mark the four bands of the spectra (blue, red, cyan, and pink). Black arrows indicate the winding direction of the quasi-energies with k varying from 0 to 2π . The parameters are $\theta_2 = 0.2\pi, 0.3\pi, 0.4\pi, 0.5\pi,$ and 0.6π from (b) to (f), with $\alpha_a = \alpha_b = 3$ and $\theta_1 = 0.2$ for all panels.

bulk sites and edge sites. In Supplemental Materials, we even add an example where reversed NHSE in our quantum walk system can be observed using only two unit cells.

Summary.- We have shown that a coherent coupling between two 1D non-Hermitian chains can lead to direction reversal of NHSE for all the eigenmodes. We have demonstrated this concept using both the spatial profile of stationary solutions, as well as time evolution dynamics on a quantum walk platform within reach of current experiments. In our first model, the common and individual direction of NHSE is obvious, as observed from the non-reciprocal hopping on the two individual chains, yet a coupling between them yields a population accumulation along the reversed direction. This intriguing phenomenon is interpreted in terms of the interference between multiple hopping pathways and explained quantitatively via an adiabatic/hybridized representation. In our second working model aiming at an experimental proposal to observe reversed NHSE on the dynamics level, two individual chains hosting a quantum walker have the same preferred direction of particle transport, yet an interchain hopping can again reverse the direction of particle transport. In both models, we have witnessed how a physical phenomenon analogous to ANM may emerge in contexts or experimental platforms of non-Hermitian physics. Our findings should also offer useful schemes to manipulate the NHSE by tuning the coherent coupling between individual subsystems. It should be stimulating to extend our findings to higher dimensions, where NHSE becomes a rather universal property of non-Hermitian systems, with the boundary localization behavior of bulk eigenmodes

strongly dependent on the system's geometry [58].

Acknowledgements.— L. L. would like to thank Zhihuang Luo and Zhenhua Yu for helpful discussion. L. L. acknowledges funding support by the National Natural Science Foundation of China (12104519) and the Guangdong Basic and Applied Basic Research Foundation (2020A1515110773). J. G. acknowledges support from Singapore National Research Foundation (Grant No. NRF-NRFI2017-04).

Supplementary Materials for “Direction reversal of non-Hermitian skin effect via coherent coupling”

PERTURBATIVE GBZ SOLUTION FOR TWO COUPLED HATANO-NELSON CHAINS

To quantitatively unveil the reversed NHSE, we solve the corresponding generalized Brillouin zone (GBZ) of two coupled Hatano-Nelson chains through a perturbative calculation. The Hamiltonian in momentum space reads

$$h(k) = \begin{pmatrix} 2t_a \cos(k - i\alpha_a) + \mu & t_\perp \\ t_\perp & 2t_b \cos(k - i\alpha_b) - \mu \end{pmatrix}. \quad (\text{S1})$$

For large t_\perp , we may take $h_0 = t_\perp \sigma_x$ as the unperturbed Hamiltonian, and the rest terms $h'(k) = h(k) - h_0$ as perturbations. The first-order perturbation of the energies are given by

$$\delta E_\pm(k) = \langle \psi_\pm | h'(k) | \psi_\pm \rangle$$

with ψ_\pm the two eigenvectors of h_0 . Here we have $\delta E_+ = \delta E_- := \delta E$, and the two branches of eigenmodes are distinguished by their unperturbed eigenenergies $E_\pm^0 = \pm t_\perp$ plus the perturbation, i.e.

$$E_\pm(k) \approx \delta E(k) \pm t_\perp.$$

To obtain the GBZ of our model, we introduce a complex deformation of the crystal momentum, $k \rightarrow k + i\kappa$. According to the non-Bloch band theory [6, 7], the GBZ is given by certain values of κ (possibly k -dependent) so that each pair of eigenmodes with different k have the same eigenenergies. Note that in our model, the k -dependency of eigenenergies appear only in the first-order perturbation $\delta E(k)$, which is the same for $E_\pm(k)$. It means that the two bands are described by the same GBZ, determined solely by $\delta E(k)$ with the complex deformation of k . With some straightforward calculation, we obtain

$$\delta E(k + i\kappa) = f_r \cos k + i f_i \sin k, \quad (\text{S2})$$

$$f_r = \left(t_a \frac{e^{-\kappa} e^{\alpha_a} + e^\kappa e^{-\alpha_a}}{2} + t_b \frac{e^{-\kappa} e^{\alpha_b} + e^\kappa e^{-\alpha_b}}{2} \right),$$

$$f_i = \left(t_a \frac{e^{-\kappa} e^{\alpha_a} - e^\kappa e^{-\alpha_a}}{2} + t_b \frac{e^{-\kappa} e^{\alpha_b} - e^\kappa e^{-\alpha_b}}{2} \right). \quad (\text{S3})$$

We can see that $\delta E(k + i\kappa)$ has its real part proportional to $\cos k$, i.e. taking the same value at $\pm k$, and its imaginary part proportional to $\sin k$, i.e. taking the same value at $\pi/2 \pm k$. Therefore, we may have $\delta E(k + i\kappa)$ taking the same value at different k only when $f_r f_i = 0$ [59], which leads to

$$e^{4\kappa} = \left(\frac{t_a e^{\alpha_a} + t_b e^{\alpha_b}}{t_a e^{-\alpha_a} + t_b e^{-\alpha_b}} \right)^2, \quad \kappa = \ln \sqrt{\left| \frac{t_a e^{\alpha_a} + t_b e^{\alpha_b}}{t_a e^{-\alpha_a} + t_b e^{-\alpha_b}} \right|}. \quad (\text{S4})$$

For $\alpha_{a,b} > 0$, the direction reversal of NHSE occurs when $\kappa < 0$, which leads to the same result as that in the main text.

EXTENSIONS OF THE TWO COUPLED HATANO-NELSON CHAINS

Energy offset between the two chains

The model of two coupled Hatano-Nelson chains considered in the main text contains an energy offset between the two chains, labeled as $\mu_a = -\mu_b = \mu$, which does not appear in the first-order perturbation correction. Physically, μ tends to separate the two chains, making it more difficult for their eigensolutions to hybridize with each other. Thus the required t_\perp for entering the regime of reversed NHSE shall increase with μ . As seen in Fig. S1, the critical value of t_\perp for the system to enter the regime of reversed NHSE, denoted as $t_{\perp,c}$, exhibits a roughly linear dependence on μ for $\mu \gtrsim 1$.

Off-diagonal interchain couplings

In the coupled Hatano-Nelson chains discussed in the main text, the direction reversal of NHSE occurs only when t_a and t_b take opposite signs, which is not a necessary condition in more general scenarios. To see this, here we consider an example with

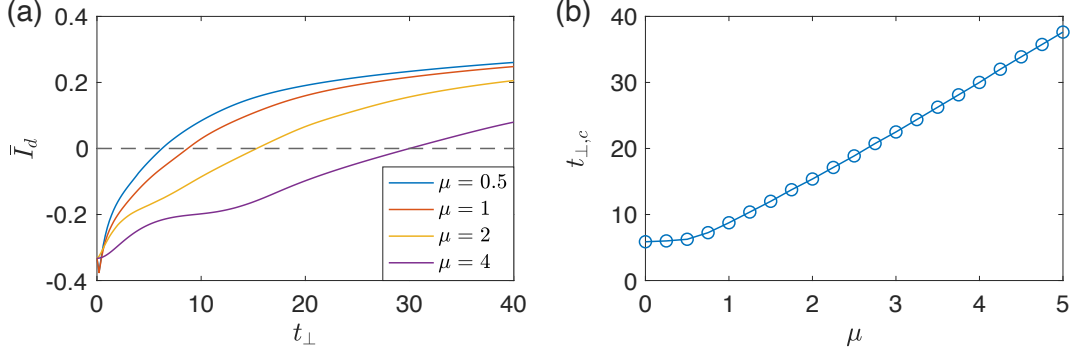


FIG. S1. (a) The average directional inverse participation ratio (dIPR) over all eigenmodes of two coupled Hatano-Nelson chains, for several different values of μ . See Eq. (3) in the main text for the definition of dIPR. The transition between normal and reversed NHSE can be identified with $\bar{I}_d = 0$, where the eigenmodes have a balanced distribution toward the two ends of the system. (b) The critical value of the interchain couplings, $t_{\perp,c}$, given by $\bar{I}_d(t_{\perp,c}) = 0$, i.e. the crossing between the solid and dash lines in (a). Other parameters are $t_a = 0.75$, $t_b = -1$, $\alpha_a = 0.5$, $\alpha_b = 0.2$.

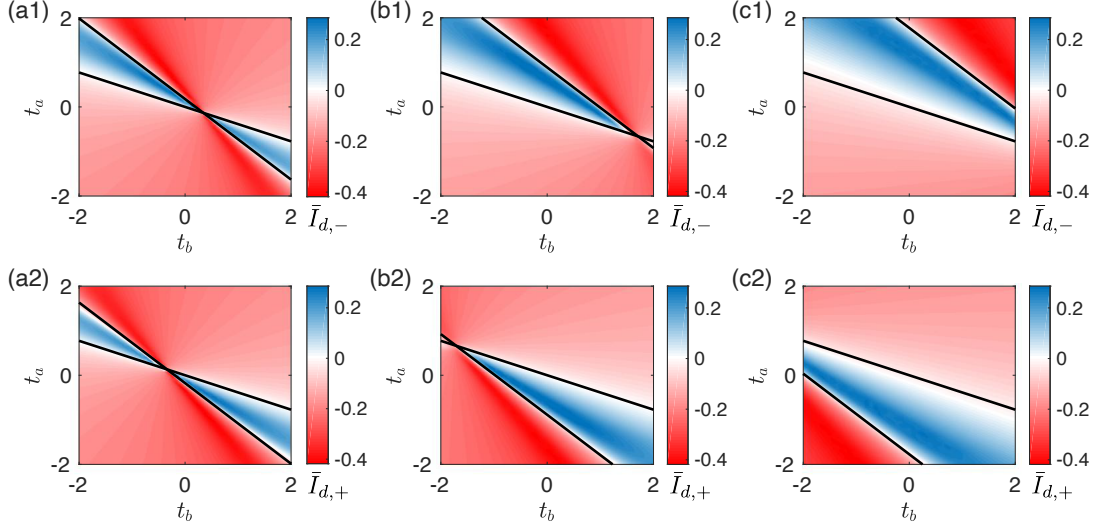


FIG. S2. Phase diagrams with color indicating the directional IPR $\bar{I}_{d,\pm}$ at $t_\perp = 30$ with additional off-diagonal interchain couplings (a) $t_2 = 0.2$, (b) $t_2 = 1$, and (c) $t_2 = 2$. Black lines are obtained from the perturbation results of Eqs. (S11) and (S12). Other parameters are $\alpha_a = 0.5$, $\alpha_b = 0.2$, and $\mu_a = -\mu_b = 0.5$.

extra off-diagonal couplings added to the model, described by

$$\hat{H}_2 = \sum_x \frac{t_2}{2} \hat{b}_x^\dagger \hat{a}_{x+1} + \frac{t_2}{2} \hat{b}_x^\dagger \hat{a}_{x-1} + \text{h.c.} \quad (\text{S5})$$

with h.c. denoting the Hermitian conjugate. The Hamiltonian of the system in momentum space now reads

$$h(k) = \begin{pmatrix} 2t_a \cos(k - i\alpha_a) + \mu & t_\perp + t_2 \cos k \\ t_\perp + t_2 \cos k & 2t_b \cos(k - i\alpha_b) - \mu \end{pmatrix}. \quad (\text{S6})$$

Similar to the previous case, here we take the term of t_\perp as the unperturbed Hamiltonian. The first-order perturbation is now given by

$$\delta E^\pm = t_a \cos(k - i\alpha_a) + t_b \cos(k - i\alpha_b) \pm t_2 \cos k. \quad (\text{S7})$$

With the complex deformation $k \rightarrow k + i\kappa$, we have

$$\delta E^\pm = f_r^\pm \cos k + i f_i^\pm \sin k, \quad (\text{S8})$$

$$f_r^\pm = \left(t_a \frac{e^{-\kappa} e^{\alpha_a} + e^\kappa e^{-\alpha_a}}{2} + t_b \frac{e^{-\kappa} e^{\alpha_b} + e^\kappa e^{-\alpha_b}}{2} \pm t_2 \frac{e^{-\kappa} + e^\kappa}{2} \right),$$

$$f_i^\pm = \left(t_a \frac{e^{-\kappa} e^{\alpha_a} - e^\kappa e^{-\alpha_a}}{2} + t_b \frac{e^{-\kappa} e^{\alpha_b} - e^\kappa e^{-\alpha_b}}{2} \pm t_2 \frac{e^{-\kappa} - e^\kappa}{2} \right). \quad (\text{S9})$$

Note that here the two bands have different dependencies on k , therefore we shall also rewrite κ as κ_\pm for the two bands. Requiring $f_r^\pm f_i^\pm = 0$, we obtained

$$e^{4\kappa_\pm} = \left(\frac{t_a e^{\alpha_a} + t_b e^{\alpha_b} \pm t_2}{t_a e^{-\alpha_a} + t_b e^{-\alpha_b} \pm t_2} \right)^2,$$

$$\kappa_\pm = \ln \sqrt{\left| \frac{t_a e^{\alpha_a} + t_b e^{\alpha_b} \pm t_2}{t_a e^{-\alpha_a} + t_b e^{-\alpha_b} \pm t_2} \right|}. \quad (\text{S10})$$

The phase boundaries between normal and reversed NHSE for each band are given by $\kappa_\pm = 0$, which leads to

$$t_a = \frac{-t_b(e^{\alpha_b} - e^{-\alpha_b})}{e^{\alpha_a} - e^{-\alpha_a}} \text{ and } t_a = \frac{-t_b(e^{\alpha_b} + e^{-\alpha_b}) - 2t_2}{e^{\alpha_a} + e^{-\alpha_a}}, \quad (\text{S11})$$

and $\kappa_- = 0$, which leads to

$$t_a = \frac{-t_b(e^{\alpha_b} - e^{-\alpha_b})}{e^{\alpha_a} - e^{-\alpha_a}} \text{ and } t_a = \frac{-t_b(e^{\alpha_b} + e^{-\alpha_b}) + 2t_2}{e^{\alpha_a} + e^{-\alpha_a}}. \quad (\text{S12})$$

The results for several different values of t_2 are shown in Fig. S2, together with the average directional IPR of the two bands, denoted as $\bar{I}_{d,\pm}$ respectively. From this result, we can see that there are two interesting consequences due to the presence of t_2 .

(i) Since now $\kappa_+ \neq \kappa_-$, it is possible to have the reversed non-reciprocal accumulation in only one band, i.e. for exactly half of the eigenmodes. In this way, the normal and reversed non-reciprocal accumulations are separated by a large energy gap as the two bands have eigenenergies around $\pm t_\perp$ respectively.

(ii) It is now also possible to have the reversed NHSE even when t_a and t_b take the same sign, which is impossible for the case with only t_\perp (i.e. $t_2 = 0$). This is because t_2 takes different signs in determining κ_\pm for the two bands, and it is possible to have one of κ_\pm changing sign by tuning t_2 . For example, in Fig. S2(c) with $t_2 = 2$, the reversed NHSE (denoted by blue color) is seen when $t_{a,b} > 0$ for “-” band, and when $t_{a,b} < 0$ for “+” band.

DETAILS OF THE TWO-CHAIN QUANTUM WALK

The Floquet operators governing the quantum walk in the main text,

$$U_0 = R(\theta_1) S_2 R(\theta_2 + \theta_3) M R(\theta_2 + \theta_3) S_1 R(\theta_1), \quad (\text{S13})$$

$$U = R(\theta_1) S_2 R(\theta_2) S_4 R(\theta_3) M R(\theta_3) S_3 R(\theta_2) S_1 R(\theta_1), \quad (\text{S14})$$

are explicitly given by

$$R(\theta) = \sum_{x=-N}^N \sum_{s=a,b} |s, x\rangle \langle s, x| \otimes e^{-i\lambda_s \theta \sigma_y / 2}, \quad M = \sum_{x=-N}^N \sum_{s=a,b} |s, x\rangle \langle s, x| \otimes (|\downarrow\rangle \langle \downarrow| + e^{-\alpha_s} |\uparrow\rangle \langle \uparrow|),$$

$$S_1 = \sum_{x=-N}^N \sum_{s=a,b} (|s, x\rangle \langle s, x| \otimes |\downarrow\rangle \langle \downarrow| + |s, x+1\rangle \langle s, x+1| \otimes |\uparrow\rangle \langle \uparrow|), \quad S_2 = \sum_{x=-N}^N \sum_{s=a,b} (|s, x-1\rangle \langle s, x-1| \otimes |\downarrow\rangle \langle \downarrow| + |s, x\rangle \langle s, x| \otimes |\uparrow\rangle \langle \uparrow|),$$

$$S_3 = \sum_{x=-N}^N \sum_{s,\bar{s}=a,b} (|s, x\rangle \langle \bar{s}, x| \otimes |\uparrow\rangle \langle \uparrow| + |s, x\rangle \langle s, x| \otimes |\downarrow\rangle \langle \downarrow|), \quad S_4 = \sum_{x=-N}^N \sum_{s,\bar{s}=a,b} (|s, x\rangle \langle \bar{s}, x| \otimes |\downarrow\rangle \langle \downarrow| + |s, x\rangle \langle s, x| \otimes |\uparrow\rangle \langle \uparrow|).$$

with $s = a, b$ denoting the two chains, x the site index, and $\lambda_a = 1$ and $\lambda_b = -1$.

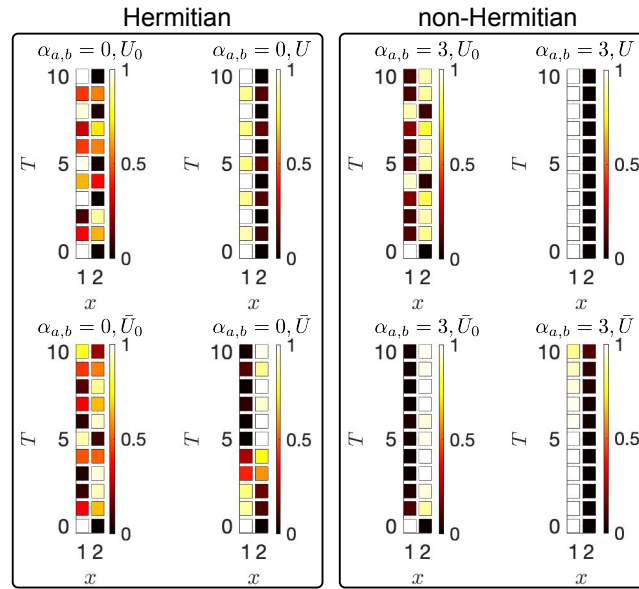


FIG. S3. The normalized spatial distribution $\rho(x)$ [or $\rho_0(x)$, $\bar{\rho}(x)$, $\bar{\rho}_0(x)$] for a quantum walk with two unit cells, i.e. $x = 1$ or 2 . The initial state is prepared as $|\Psi_{\text{ini}}\rangle = |a, 1\rangle \otimes |\uparrow\rangle$. From left to right, the results are obtained with the system being (i) Hermitian and decoupled; (ii) Hermitian and coupled; (iii) non-Hermitian and decoupled, (iv) non-Hermitian and coupled. The parameters are $\alpha_a = \alpha_b = 0$ and $\alpha_a = \alpha_b = 3$ for Hermitian and non-Hermitian cases respectively.

QUANTUM WALK IN A SYSTEM WITH TWO UNIT CELLS

Since the NHSE describes a unidirectional transport of the (quasi-)particles or wave packets, direction reversal of NHSE in principle can manifest itself in very small systems, as long as a direction can be defined. Specifically, we consider the quantum walk discussed in the main text in a system with the position x only takes 1 or 2, i.e. 4 qubits for the two chains. To distinguish the left- and right- propagations, the system must be under the ‘‘OBC’’, where the shift operators S_1 and S_2 are also non-unitary. That is, S_1 will eliminate the (quasi-)particle at $|s, 2\rangle \otimes |\uparrow\rangle$, since $x = 2 + 1$ is not included in the system. For the same reason, S_2 will eliminate the amplitude at $|s, 1\rangle \otimes |\downarrow\rangle$. Therefore in such a small system, whether S_1 or S_2 acts first in the Floquet operator may also affect the results. To this end, we also consider another two sets of Floquet operators,

$$\begin{aligned}\bar{U} &= R(\theta_1)S_1R(\theta_2)S_4R(\theta_3)MR(\theta_3)S_3R(\theta_2)S_2R(\theta_1), \\ \bar{U}_0 &= R(\theta_1)S_1R(\theta_2 + \theta_3)MR(\theta_2 + \theta_3)S_2R(\theta_1),\end{aligned}\tag{S15}$$

where the roles of S_1 and S_2 are exchanged when compared with U and U_0 .

By comparing the dynamical evolutions governed by these four Floquet operators (U , U_0 , \bar{U} , and \bar{U}_0) with or without the non-Hermitian loss, the direction reversal of NHSE induced by the interchain couplings can be justified even in this two-unit-cell system, as demonstrated in Fig. S3. Below we summarize the results. Starting from the left of Fig. S3,

(i) in the first column, we choose $\alpha_{a,b} = 0$, and consider the quantum walks without the interchain couplings, governed by U_0 and \bar{U}_0 respectively. There is no non-reciprocal pumping since there is no gain or loss in the system.

(ii) in the second column, we choose $\alpha_{a,b} = 0$, and consider the quantum walks with the interchain couplings, governed by U and \bar{U} respectively. Even without any gain or loss in the system, we still observe some non-reciprocal accumulations. However, we can see that U and \bar{U} (with $S_{1,2}$ exchanging their roles) induce different accumulating directions, showing that this is not the NHSE, but a consequence of the boundary effect induced by S_1 and S_2 .

(iii) in the third column, we choose $\alpha_{a,b} = 3$, and consider the same quantum walks as that of the first column. We see a clear non-reciprocal accumulation from $x = 1$ to $x = 2$, for both Floquet operators. Therefore we conclude that this non-reciprocal accumulation reflects the NHSE, rather than the boundary effect induced by S_1 and S_2 .

(iv) in the last column, we choose $\alpha_{a,b} = 3$, and consider the same quantum walks as that of the second column. A clear non-reciprocal accumulation is seen from $x = 2$ to $x = 1$, also for both Floquet operators. Compared with (iii), we can see that the direction of population accumulation is reversed when introducing S_3 and S_4 , representing the direction reversal of NHSE induced by interchain couplings.

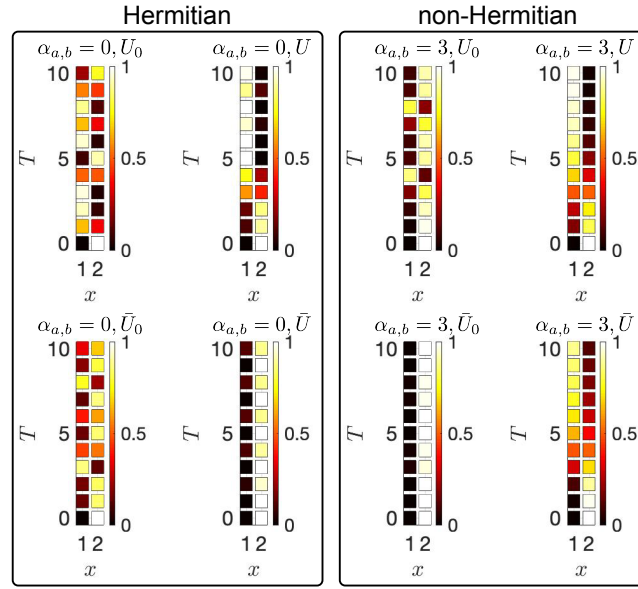


FIG. S4. The normalized spatial distribution $\rho(x)$ [or $\rho_0(x)$, $\bar{\rho}(x)$, $\bar{\rho}_0(x)$] for a quantum walk with two unit cells, i.e. $x = 1$ or 2 . The initial state is prepared as $\Psi_{\text{ini}} = |a, 2\rangle \otimes |\uparrow\rangle$, which is different from that in Fig. S3. From left to right, the results are obtained with (i) Hermitian and decoupled; (ii) Hermitian and coupled; (iii) non-Hermitian and decoupled, (iv) non-Hermitian and coupled. Hermitian and non-Hermitian cases correspond to $\alpha_a = \alpha_b = 0$ and $\alpha_a = \alpha_b = 3$ respectively.

In Fig. S4, keeping parameters the same with those in Fig. S3, we present the results with a different initial state $\Psi_{\text{ini}} = |a, 2\rangle \otimes |\uparrow\rangle$ and we observe the same phenomena as shown in Fig. S3.

* lilh56@mail.sysu.edu.cn

† senmu@u.nus.edu

‡ phygj@nus.edu.sg

- [1] Carl M. Bender and Stefan Boettcher, “Real spectra in non-hermitian hamiltonians having pt symmetry,” *Phys. Rev. Lett.* **80**, 5243–5246 (1998).
- [2] Carl M Bender, “Making sense of non-hermitian hamiltonians,” *Reports on Progress in Physics* **70**, 947 (2007).
- [3] Ingrid Rotter, “A non-hermitian hamilton operator and the physics of open quantum systems,” *Journal of Physics A: Mathematical and Theoretical* **42**, 153001 (2009).
- [4] Yuto Ashida, Zongping Gong, and Masahito Ueda, “Non-hermitian physics,” *Advances in Physics* **69**, 249–435 (2020).
- [5] VM Martinez Alvarez, JE Barrios Vargas, and LEF Foa Torres, “Non-hermitian robust edge states in one dimension: Anomalous localization and eigenspace condensation at exceptional points,” *Phys. Rev. B* **97**, 121401 (2018).
- [6] Shunyu Yao and Zhong Wang, “Edge states and topological invariants of non-hermitian systems,” *Phys. Rev. Lett.* **121**, 086803 (2018).
- [7] Kazuki Yokomizo and Shuichi Murakami, “Non-bloch band theory of non-hermitian systems,” *Physical review letters* **123**, 066404 (2019).
- [8] Ching Hua Lee and Ronny Thomale, “Anatomy of skin modes and topology in non-hermitian systems,” *Phys. Rev. B* **99**, 201103 (2019).
- [9] Shunyu Yao, Fei Song, and Zhong Wang, “Non-hermitian chern bands,” *Phys. Rev. Lett.* **121**, 136802 (2018).
- [10] Fei Song, Shunyu Yao, and Zhong Wang, “Non-hermitian skin effect and chiral damping in open quantum systems,” *Physical review letters* **123**, 170401 (2019).
- [11] Dan S. Borgnia, Alex Jura Kruchkov, and Robert-Jan Slager, “Non-hermitian boundary modes and topology,” *Phys. Rev. Lett.* **124**, 056802 (2020).
- [12] Nobuyuki Okuma, Kohei Kawabata, Ken Shiozaki, and Masatoshi Sato, “Topological origin of non-hermitian skin effects,” *Phys. Rev. Lett.* **124**, 086801 (2020).
- [13] Kai Zhang, Zhesen Yang, and Chen Fang, “Correspondence between winding numbers and skin modes in non-hermitian systems,” *Phys. Rev. Lett.* **125**, 126402 (2020).
- [14] Ching Hua Lee, Linhu Li, and Jiangbin Gong, “Hybrid higher-order skin-topological modes in nonreciprocal systems,” *Phys. Rev. Lett.* **123**, 016805 (2019).
- [15] Linhu Li, Ching Hua Lee, and Jiangbin Gong, “Topological switch for non-hermitian skin effect in cold-atom systems with loss,” *Physical Review Letters* **124**, 250402 (2020).

- [16] Linhu Li, Ching Hua Lee, Sen Mu, and Jiangbin Gong, “Critical non-hermitian skin effect,” *Nature communications* **11** (2020).
- [17] Yifei Yi and Zhesen Yang, “Non-hermitian skin modes induced by on-site dissipations and chiral tunneling effect,” *Phys. Rev. Lett.* **125**, 186802 (2020).
- [18] Ming Lu, Xiao-Xiao Zhang, and Marcel Franz, “Magnetic suppression of non-hermitian skin effects,” *Phys. Rev. Lett.* **127**, 256402 (2021).
- [19] Kuangyin Deng and Benedetta Flebus, “Non-hermitian skin effect in magnetic systems,” 2109.01711v3.
- [20] Yi Peng, Jianwen Jie, Dapeng Yu, and Yucheng Wang, “Manipulating non-hermitian skin effect via electric fields,” 2201.10318v2.
- [21] Hui Jiang, Li-Jun Lang, Chao Yang, Shi-Liang Zhu, and Shu Chen, “Interplay of non-hermitian skin effects and anderson localization in nonreciprocal quasiperiodic lattices,” *Physical Review B* **100**, 054301 (2019).
- [22] Stefano Longhi, “Topological phase transition in non-hermitian quasicrystals,” *Physical Review Letters* **122**, 237601 (2019).
- [23] Qi-Bo Zeng, Yan-Bin Yang, and Yong Xu, “Topological phases in non-hermitian aubry-andré-harper models,” *Physical Review B* **101**, 020201 (2020).
- [24] Linhu Li, Ching Hua Lee, and Jiangbin Gong, “Impurity induced scale-free localization,” *Communications Physics* **4**, 1–9 (2021).
- [25] Cui-Xian Guo, Chun-Hui Liu, Xiao-Ming Zhao, Yanxia Liu, and Shu Chen, “Exact solution of non-hermitian systems with generalized boundary conditions: Size-dependent boundary effect and fragility of the skin effect,” *Phys. Rev. Lett.* **127**, 116801 (2021).
- [26] Yanxia Liu, Yumeng Zeng, Linhu Li, and Shu Chen, “Exact solution of the single impurity problem in nonreciprocal lattices: Impurity-induced size-dependent non-hermitian skin effect,” *Phys. Rev. B* **104**, 085401 (2021).
- [27] Balaganchi A. Bhargava, Ion Cosma Fulga, Jeroen van den Brink, and Ali G. Moghaddam, “Non-hermitian skin effect of dislocations and its topological origin,” *Phys. Rev. B* **104**, L241402 (2021).
- [28] Frank Schindler and Abhinav Prem, “Dislocation non-hermitian skin effect,” *Phys. Rev. B* **104**, L161106 (2021).
- [29] Xiao-Qi Sun, Penghao Zhu, and Taylor L. Hughes, “Geometric response and disclination-induced skin effects in non-hermitian systems,” *Phys. Rev. Lett.* **127**, 066401 (2021).
- [30] Clara C Wanjura, Matteo Brunelli, and Andreas Nunnenkamp, “Topological framework for directional amplification in driven-dissipative cavity arrays,” *Nature communications* **11**, 1–13 (2020).
- [31] Clara C. Wanjura, Matteo Brunelli, and Andreas Nunnenkamp, “Correspondence between non-hermitian topology and directional amplification in the presence of disorder,” *Phys. Rev. Lett.* **127**, 213601 (2021).
- [32] Lei Xiao, Tianshu Deng, Kunkun Wang, Gaoyan Zhu, Zhong Wang, Wei Yi, and Peng Xue, “Non-hermitian bulk–boundary correspondence in quantum dynamics,” *Nature Physics* **16**, 761 (2020).
- [33] Lei Xiao, Tianshu Deng, Kunkun Wang, Zhong Wang, Wei Yi, and Peng Xue, “Observation of non-bloch parity-time symmetry and exceptional points,” *Physical Review Letters* **126**, 230402 (2021).
- [34] Kunkun Wang, Tianyu Li, Lei Xiao, Yiwen Han, Wei Yi, and Peng Xue, “Detecting non-bloch topological invariants in quantum dynamics,” *Physical Review Letters* **127**, 270602 (2021).
- [35] Brian J Keay, Stefan Zeuner, SJ Allen Jr, Kevin D Maranowski, Art C Gossard, Uddalak Bhattacharya, and Marc JW Rodwell, “Dynamic localization, absolute negative conductance, and stimulated, multiphoton emission in sequential resonant tunneling semiconductor superlattices,” *Physical review letters* **75**, 4102 (1995).
- [36] Ethan H Cannon, Feodor V Kusmartsev, Kirill N Alekseev, and David K Campbell, “Absolute negative conductivity and spontaneous current generation in semiconductor superlattices with hot electrons,” *Physical Review Letters* **85**, 1302 (2000).
- [37] Ralf Eichhorn, Peter Reimann, and Peter Hänggi, “Brownian motion exhibiting absolute negative mobility,” *Physical review letters* **88**, 190601 (2002).
- [38] Ralf Eichhorn, Peter Reimann, and Peter Hänggi, “Paradoxical motion of a single brownian particle: Absolute negative mobility,” *Physical Review E* **66**, 066132 (2002).
- [39] Lukasz Machura, Marcin Kostur, Peter Talkner, Jerzy Łuczka, and Peter Hänggi, “Absolute negative mobility induced by thermal equilibrium fluctuations,” *Physical review letters* **98**, 040601 (2007).
- [40] J Nagel, David Speer, T Gaber, A Sterck, R Eichhorn, Peter Reimann, K Ilin, M Siegel, D Koelle, and R Kleiner, “Observation of negative absolute resistance in a josephson junction,” *Physical review letters* **100**, 217001 (2008).
- [41] Alexandra Ros, Ralf Eichhorn, Jan Regtmeier, Thanh Tu Duong, Peter Reimann, and Dario Anselmetti, “Absolute negative particle mobility,” *Nature* **436**, 928–928 (2005).
- [42] David Reguera, A Luque, Poornachandra Sekhar Burada, Gerhard Schmid, JM Rubi, and Peter Hänggi, “Entropic splitter for particle separation,” *Physical Review Letters* **108**, 020604 (2012).
- [43] Aleksandra Słapik, Jerzy Łuczka, Peter Hänggi, and Jakub Spiechowicz, “Tunable mass separation via negative mobility,” *Physical Review Letters* **122**, 070602 (2019).
- [44] Pulak K Ghosh, Peter Hänggi, Fabio Marchesoni, and Franco Nori, “Giant negative mobility of janus particles in a corrugated channel,” *Physical Review E* **89**, 062115 (2014).
- [45] A Sarracino, F Cecconi, A Puglisi, and A Vulpiani, “Nonlinear response of inertial tracers in steady laminar flows: Differential and absolute negative mobility,” *Physical review letters* **117**, 174501 (2016).
- [46] Sebastian Weidemann, Mark Kremer, Tobias Helbig, Tobias Hofmann, Alexander Stegmaier, Martin Greiter, Ronny Thomale, and Alexander Szameit, “Topological funneling of light,” *Science* **368**, 311–314 (2020).
- [47] Wen-Tan Xue, Ming-Rui Li, Yu-Min Hu, Fei Song, and Zhong Wang, “Simple formulas of directional amplification from non-bloch band theory,” *Physical Review B* **103**, L241408 (2021).
- [48] Martin Brandenbourger, Xander Locsin, Edan Lerner, and Corentin Coulais, “Non-reciprocal robotic metamaterials,” *Nature communications* **10**, 1–8 (2019).
- [49] T Helbig, T Hofmann, S Imhof, M Abdelghany, T Kiessling, LW Molenkamp, CH Lee, A Szameit, M Greiter, and R Thomale, “Generalized bulk-boundary correspondence in non-hermitian topoelectrical circuits,” *Nature Physics* **16**, 747–750 (2020).
- [50] Ananya Ghatak, Martin Brandenbourger, Jasper van Wezel, and Corentin Coulais, “Observation of non-hermitian topology and its

- bulk–edge correspondence in an active mechanical metamaterial,” *Proceedings of the National Academy of Sciences* **117**, 29561–29568 (2020).
- [51] Tobias Hofmann, Tobias Helbig, Frank Schindler, Nora Salgo, Marta Brzezińska, Martin Greiter, Tobias Kiessling, David Wolf, Achim Vollhardt, Anton Kabaši, *et al.*, “Reciprocal skin effect and its realization in a topoelectrical circuit,” *Physical Review Research* **2**, 023265 (2020).
- [52] Qian Liang, Dizhou Xie, Zhaoli Dong, Haowei Li, Hang Li, Bryce Gadway, Wei Yi, and Bo Yan, “Observation of non-hermitian skin effect and topology in ultracold atoms,” (), 2201.09478v1.
- [53] Naomichi Hatano and David R. Nelson, “Localization transitions in non-hermitian quantum mechanics,” *Phys. Rev. Lett.* **77**, 570–573 (1996).
- [54] Hui-Qiang Liang, Sen Mu, Jiangbin Gong, and Linhu Li, “Anomalous hybridization of spectral winding topology in quantized steady-state responses,” (), 2112.05191v1.
- [55] Sen Mu, Longwen Zhou, Linhu Li, and Jiangbin Gong, “Non-hermitian pseudo mobility edge in a coupled chain system,” 2111.11914v1.
- [56] Fei Song, Shunyu Yao, and Zhong Wang, “Non-hermitian topological invariants in real space,” *Physical Review Letters* **123**, 246801 (2019).
- [57] Li Zhang, Yihao Yang, Yong Ge, Yi-Jun Guan, Qiaolu Chen, Qinghui Yan, Fujia Chen, Rui Xi, Yuanzhen Li, Ding Jia, *et al.*, “Acoustic non-hermitian skin effect from twisted winding topology,” *Nature communications* **12**, 6297 (2021).
- [58] Kai Zhang, Zhesen Yang, and Chen Fang, “Universal non-hermitian skin effect in two and higher dimensions,” arXiv preprint arXiv:2102.05059 (2021).
- [59] Linhu Li, Ching Hua Lee, and Jiangbin Gong, “Geometric characterization of non-hermitian topological systems through the singularity ring in pseudospin vector space,” *Physical Review B* **100**, 075403 (2019).